Sorting of multiple molecular species on cell membranes

Sorting of multiple molecular species on cell membranes

Andrea Piras,[1,2,3,4,*] Elisa Floris,[2,5,*] Luca Dall'Asta,[2,3,6,†] and Andrea Gamba[2,3,5,‡]

[1]*Candiolo Cancer Institute, FPO-IRCCS, Strada Provinciale 142, km 3.95, 10060 Candiolo, Italy*
[2]*Institute of Condensed Matter Physics and Complex Systems, Department of Applied Science and Technology, Politecnico di Torino, Corso Duca degli Abruzzi 24, 10129 Turin, Italy*
[3]*Italian Institute for Genomic Medicine (IIGM), Strada Provinciale 142, km 3.95, 10060 Candiolo, Italy*
[4]*Department of Oncology, University of Turin, 10060 Candiolo, Italy*
[5]*Istituto Nazionale di Fisica Nucleare (INFN), Sezione di Torino, Via Pietro Giuria 1, 10125 Torino, Italy*
[6]*Collegio Carlo Alberto, Piazza Arbarello 8, 10122, Torino, Italy*

(Received 24 January 2023; revised 12 May 2023; accepted 5 June 2023; published 3 August 2023)

Eukaryotic cells maintain their inner order by a hectic process of sorting and distillation of molecular factors taking place on their lipid membranes. A similar sorting process is implied in the assembly and budding of enveloped viruses. To understand the properties of this molecular sorting process, we have recently proposed a physical model [Zamparo *et al.*, Phys. Rev. Lett. **126**, 088101 (2021)], based on (1) the phase separation of a single, initially dispersed molecular species into spatially localized sorting domains on the lipid membrane and (2) domain-induced membrane bending leading to the nucleation of submicrometric lipid vesicles, naturally enriched in the molecules of the engulfed sorting domain. The analysis of the model showed the existence of an optimal region of parameter space where sorting is most efficient. Here the model is extended to account for the simultaneous distillation of a pool of distinct molecular species. We find that the mean time spent by sorted molecules on the membrane increases with the heterogeneity of the pool (i.e., the number of distinct molecular species sorted) according to a simple scaling law, and that a large number of distinct molecular species can in principle be sorted in parallel on cell membranes without significantly interfering with each other. Moreover, sorting is found to be most efficient when the distinct molecular species have comparable homotypic affinities. We also consider how valence (i.e., the average number of interacting neighbors of a molecule in a sorting domain) affects the sorting process, finding that higher-valence molecules can be sorted with greater efficiency than lower-valence molecules.

DOI: 10.1103/PhysRevE.108.024401

I. INTRODUCTION

Eukaryotic cells have developed a complex mechanism of molecular distillation, allowing them to impart distinct chemical identities to a variety of inner cell organelles that host specific sets of proteins and lipids and perform specific functions [1,2]. At the basis of this process of organelle maintenance and renewal is a hectic traffic of vesicles generated through a sophisticated process of sorting of molecular factors taking place both on the outer cell membrane and on the membranes that enclose inner cell compartments. A similar process of sorting of specific molecular factors into localized membrane domains is involved in the assembly of enveloped viruses (such as HIV, SARS-CoV, and influenza) and in their budding from host cells [3–6]. We have recently proposed that molecular sorting may emerge from the combination of two fundamental physical mechanisms [7]: (1) the phase separation of a single, initially dispersed molecular species into spatially localized sorting domains and (2) domain-induced nucleation of submicrometric lipid vesicles, which then become naturally enriched in the molecules contained in the engulfed sorting domain. Based on these assumptions, we have developed a phenomenological theory, where the main control parameter is the intermolecular interaction strength which drives the phase separation process and regulates the critical size of sorting domains, which separates small, transient, "unproductive" sorting domains from larger, "productive" sorting domains destined to grow and to be ultimately extracted [7,8]. It is important to observe here that the interaction between homotypic molecules leading to their phase separation into distinct sorting domains may be either *direct*, such as in the case of the weakly adhesive electrostatic interactions between unstructured molecular regions involved in liquid-liquid phase separation [9], or *indirect*, as in the case of the effective, contactless interactions induced by enzyme-driven feedback loops involving both lipids and proteins. The latter, indirect interactions have the potential to induce diffusion-limited phase separation, originally studied in the context of cell polarity [10–16], and are involved in molecular sorting processes where the segregation of distinct molecular species in separate sorting domains is not controlled by direct homotypic intermolecular interactions [17]. In our phenomenological approach, the observable *effective interaction*

*These authors contributed equally.
†luca.dallasta@polito.it
‡andrea.gamba@polito.it

strength measures the tendency of homotypic molecules to become enriched in localized spatial regions, irrespective of the microscopic (direct or indirect) origin of the attraction [7,8]. It is important to consider here that in biological phase separation, the formation of localized domains is often driven by the action of positive feedback loops that involve several molecular factors [10–16]. The resulting phase-separated domains are thus enriched in the whole set of molecular factors that participate in each feedback loop. Distinct feedback loops lead to the formation of localized domains endowed with distinct chemical identities. To simplify the discussion, we consider here a *coarse-grained* description, where each of the distinct chemical identities emerging from phase separation is represented by a single, *representative* molecular species, such as a well-defined cargo molecule. It should be kept in mind, however, that on a real cell membrane, a domain enriched in the representative molecular species will also be enriched in a whole clan of associated molecular factors. For instance, the endocytic sorting of a cargo molecule also involves the accumulation in sorting domains of a whole set of auxiliary molecules, playing the roles of scaffolds, regulators, etc. [1,2]. In the same spirit, we consider here *effective* attractive interactions between members of homotypic representative species that may result from the participation of the representative species, together with a clan of associated molecular factors, to a common network of reinforcing feedback loops, even in the absence of any *direct* homotypic interaction.

A natural measure of the efficiency of the distillation process is the time a molecule spends on a given membrane region before being sorted and extracted: The shorter this residence time, the larger the distillation efficiency. In the steady state, the distillation process is most efficient for intermediate aggregation strengths, where both the molecular residence time and the average surface density of sorted molecules are minimal, and both are related to the incoming molecule flux through universal scaling laws [7]. The phenomenological theory reproduces well the experimental distribution of sorting domain sizes [7] and the experimental distributions of the lifetimes and maximum sizes of both productive and unproductive sorting domains [8,18].

Experimental investigations have been mainly focused on the process of sorting of single molecular species, such as transferrin receptors or low-density lipoproteins [1]. More recently, advances in imaging technologies have made it possible to elucidate aspects of the simultaneous distillation of distinct molecular species, and to directly observe their localization in distinct, separate sorting domains [19–22]. The demixing of distinct molecular species subject to attractive homotypic interactions at equilibrium is predicted by statistical physics arguments [23,24]. Here we propose an extension of the nonequilibrium theory of molecular sorting introduced in Ref. [7], where sorting of a single molecular species was considered, to the case where a plurality of distinct molecular species is sorted in parallel in the same membrane region. In this more general case, by combining theoretical arguments and lattice-gas numerical simulations, we show that the mean time sorted molecules reside on the membrane increases with the heterogeneity of the pool (i.e., the number of distinct molecular species sorted) according to a simple scaling law, and that a large number of distinct molecular species can in principle be sorted in parallel on a cell membrane without significantly interfering with each other. Moreover, sorting is found to be most efficient when distinct molecular species have comparable homotypic affinities. Since recent studies have highlighted a crucial role of valence (i.e., the average number of interacting neighbors of a molecule in a crowded homotypic domain) in driving phase separation and sorting on cell membranes [25–27], we also performed numerical simulations of the sorting of molecules with different valence, finding that higher-valence molecules can be sorted with greater efficiency.

II. PHENOMENOLOGICAL THEORY FOR THE PARALLEL SORTING OF MULTIPLE MOLECULAR SPECIES

The phenomenological theory of molecular sorting driven by phase separation previously introduced in Ref. [7] is here generalized to the case of the parallel distillation of $N > 1$ noninteracting molecular species. The theory describes "cargo" molecules continuously injected into the lipid membrane in random positions, and then laterally diffusing on the membrane. Attractive (direct or indirect) interactions between homotypic molecules (i.e., molecules belonging to the same species) can lead to the formation of multiple sorting domains enriched in the molecules of a particular species, thus inducing a natural *demixing* process. Effective homotypic attractive interactions drive the growth of approximately circular, homotypic sorting domains by the absorption of freely diffusing molecules, that form a sort of two-dimensional "gas" of molecules surrounding the growing domains. In the formation of a domain from a random fluctuation of a free molecule gas of large enough density, the energetically unfavorable creation of a domain-gas interface is accompanied by the energetically favorable creation of a homogeneous domain bulk. There exists therefore a critical size A_c, such that subcritical domains of size $A < A_c$ are unstable and tend to dissolve, since the interface-associated cost dominates, while supercritical domains of size $A > A_c$ tend to grow indefinitely [28,29]. When a supercritical domain reaches a characteristic area A_E, it is extracted from the membrane system through the formation of a separate lipid vesicle, that thus becomes naturally enriched in the molecular species contained in the engulfed domain. It is worth observing here that in real cells, the process of vesicle growth and budding is highly complex and requires the intervention of multiple molecular factors in a precise temporal sequence [1,30,31], while in our abstract, coarse-grained model, we retain information only about the average size of ultimately extracted vesicles, whose diameter is of the order of 100 nm [30].

The self-organized process of parallel distillation of N molecular species defines a nonequilibrium steady state, whose statistical properties are determined by the incoming flux of molecules and by the strength of the effective attractive interaction between homotypic molecules diffusing on the given membrane region. In the low-density regime, the process of formation of domains enriched in a specific type of cargo molecule is approximately independent of the formation of domains of the other species and is regulated by the value of the critical size of sorting domains, beyond which irreversible domain growth takes place [8].

The growth of an approximately circular domain of the ith species is driven by the flux Φ_i of such molecules across the domain boundary. In the quasistationary regime, and in the limit of low-density gas and approximately absorbing domains [7], Φ_i can be computed by solving a two-dimensional Laplace equation with Dirichlet boundary conditions and circular symmetry, finding

$$\Phi_i \sim D_i\, \bar{n}_i, \tag{1}$$

where $\bar{n}_i$ is the average density of freely diffusing molecules of the ith species, and D_i is the corresponding diffusion coefficient. In the stationary regime, all particles of the ith species injected in the system are eventually absorbed by supercritical domains, therefore their flux ϕ_i obeys

$$\phi_i \sim \Phi_i\, \bar{N}_{d,i}, \tag{2}$$

where $\bar{N}_{d,i}$ is the average density of supercritical domains of the ith species.

In the nonequilibrium stationary state, the average number ϕ_i of particles of the ith species injected into the membrane system per unit time and unit area equals the analogous number of such particles leaving the system as a consequence of domain extractions. Under the assumption that supercritical domains grow irreversibly until extraction, one gets

$$\phi_i = m_i \frac{d\bar{N}_{d,i}}{dt}, \tag{3}$$

where $d\bar{N}_{d,i}/dt$ is the rate of formation of supercritical domains of the ith species per unit membrane area, and $m_i = A_E/A_{0,i}$, with $A_{0,i}$ the average area occupied by a sorted molecule in a sorting domain. The rate of formation of such domains depends on the frequency of formation of germs of new sorting domains and on the probability that those germs reach the supercritical stage. Since the formation of a domain is initiated by the encounter of two freely diffusing molecules of the ith species, the rate of domain formation has to be proportional to the square of the average free molecule density $\bar{n}_i$ [7] (for an analytical derivation, see also Ref. [8], Appendix A). Therefore, the rate of formation of supercritical domains can be expressed phenomenologically as

$$\frac{d\bar{N}_{d,i}}{dt} = C_i D_i \bar{n}_i^2, \tag{4}$$

where C_i is a dimensionless quantity representing the macroscopic, effective strength of the attractive interaction acting between homotypic molecules [7,8]. According to a general steady-state relation valid for open systems in a driven nonequilibrium stationary state, the average density of particles in the system is given by the product of the average density flux of particles and the average residence time of a particle in the system [32]. In the present case, this relation can be applied to several entities that populate the membrane in the statistically stationary state. For the total, average density ρ of molecules (both freely diffusing and bound to sorting domains) of all N species in the stationary state one has

$$\rho = \phi\, \bar{T}, \tag{5}$$

where $\bar{T}$ is the average molecule residence time on the membrane, and $\phi = \sum_{i=1}^{N} \phi_i$. This shows in particular that for fixed values of the molecular flux ϕ, the average residence time $\bar{T}$ is simply proportional to the average molecule density ρ. For the average density of freely diffusing molecules of the ith species one finds

$$\bar{n}_i = \phi_i\, \bar{T}_{f,i}, \tag{6}$$

where $\bar{T}_{f,i}$ is the average time a molecule of the ith species spends in the gas. For the average density of supercritical domains of the ith species one has

$$\bar{N}_{d,i} = \frac{d\bar{N}_{d,i}}{dt}\, \bar{T}_{d,i} = \frac{\phi_i}{m}\, \bar{T}_{d,i}, \tag{7}$$

where $\bar{T}_{d,i}$ is the average lifetime of a sorting domain. The latter, in the limit of approximately absorbing domains, is of the order of the average time a molecule of the ith species spends as a part of a sorting domain. For simplicity, we analyze here only the symmetric case, where $A_{0,i} = A_0$, $C_i = C$ and $D_i = D$ for all $i = 1, \ldots, N$, and also assume that $\bar{T}_{f,i} = \bar{T}_f$, $\bar{T}_{d,i} = \bar{T}_d$, and $\phi_i = \phi/N$ for all $i = 1, \ldots, N$. The total density of molecules in the gas is then

$$\bar{n} = \phi\, \bar{T}_f, \tag{8}$$

while the total number of supercritical domains per unit area is

$$\bar{N}_d = \phi\, \bar{T}_d/m. \tag{9}$$

Combining the relations (1)–(9), all the main quantities describing the behavior of the system in the nonequilibrium, statistically stationary state can be explicitly expressed in terms of the number of species N, the total incoming molecule flux ϕ, the extraction size $m = A_E/A_0$, the diffusivity D, and the phenomenological interaction strength C, as

$$\bar{n} \sim \left(\frac{\phi N}{m C D}\right)^{1/2}, \tag{10}$$

$$\bar{N}_d \sim \left(\frac{m C \phi N}{D}\right)^{1/2}, \tag{11}$$

$$\bar{T}_d \sim \left(\frac{m^3 C N}{D \phi}\right)^{1/2}, \tag{12}$$

$$\bar{T}_f \sim \left(\frac{N}{m C D \phi}\right)^{1/2}. \tag{13}$$

The efficiency of the molecular sorting process in the steady state is inversely proportional to the mean time of residence of a cargo molecule on the membrane, approximately given by $\bar{T} = \bar{T}_f + \bar{T}_d$. The highest efficiency is obtained when $\bar{T}$ is minimal, i.e., for

$$C \sim C_{\mathrm{opt}} \sim m^{-2}. \tag{14}$$

In this optimal regime, each molecule spends approximately the same amount of time freely diffusing in the gas and as a part of a growing domain,

$$\bar{T} \sim \bar{T}_{\mathrm{opt}} \sim \bar{T}_d \sim \bar{T}_f \sim \left(\frac{m N}{D \phi}\right)^{1/2}. \tag{15}$$

For a fixed value of the incoming flux ϕ, the mean total residence time of a molecule on the membrane increases therefore with the number of different species as $\bar{T} \sim N^{1/2}$. In the optimal regime, the average density of freely diffusing

TABLE I. Scaling laws for the average total molecule density ρ, average density of freely diffusing molecules $\bar{n}$, and average density of domains $\bar{N}_d$ in the optimal regime as a function of the number of molecular species N are reported in the first column. The corresponding theoretically predicted and numerically computed exponents are reported in the second and third columns, respectively. Numerical simulations were performed with incoming molecule flux $\phi/k_D = 10^{-5}$ on a regular square lattice, as detailed in Sec. III.

Scaling law	Theoretical	Numerical
$\rho_{\rm opt} = \phi\,\bar{T}_{\rm opt} \sim N^a$	$a = 1/2$	$a = 0.51$
$\bar{n}_{\rm opt} \sim N^b$	$b = 1/2$	$b = 0.62$
$\bar{N}_{d,{\rm opt}} \sim N^c$	$c = 1/2$	$c = 0.50$

molecules and the average density of supercritical domains behave as

$$\bar{n}_{\rm opt} \sim \left(\frac{m\,\phi\,N}{D}\right)^{1/2}, \tag{16}$$

$$\bar{N}_{d,{\rm opt}} \sim \left(\frac{\phi\,N}{m\,D}\right)^{1/2}. \tag{17}$$

From (10) and (11), it follows that also the total molecule density $\rho \sim \bar{n} + m\bar{N}_d$ scales as $\rho \sim N^{1/2}$ and is minimal for $C \sim C_{\rm opt}$. A summary of the scaling laws for the optimal regime is given in Table I. A consequence of the above relations is that even for low, fixed values of the *total* incoming molecule flux ϕ, the low-density regime, where molecules and domains of different species do not interact significantly, progressively breaks down as the number N of species increases. For very high N, the crowding of molecules of different species surrounding a domain can be expected to cause an effective decrease in the flux Φ_i at the surface, such that (1) should be modified into $\Phi_i \propto f_N D\,\bar{n}_i$, with f_N a decreasing function of N. In that case, a simple modification of the previous phenomenological arguments gives $C_{\rm opt} \sim f_N\,m^{-2}$, thus predicting that the optimal effective interaction between homotypic molecules should decrease for very large N.

A rough indication about the number of different species that can be sorted in parallel without significantly interfering with each other in the optimal sorting regime can be obtained by noticing that in the low-density regime, the interdomain half distance L has to be much larger than the extraction size $A_E^{1/2}$. Observing that $\pi\,L^2\bar{N}_d \sim 1$, and using Eq. (17), this condition translates into

$$L \sim \bar{N}_d^{-1/2} \sim \left(\frac{D\,m}{N\,\phi}\right)^{1/4} \gg A_E^{1/2}, \tag{18}$$

giving

$$N \ll \frac{D}{A_E A_0 \phi}. \tag{19}$$

Using the realistic orders of magnitude $D \sim 10^{-3}$ $\mu{\rm m}^2/{\rm s}$, $A_E \sim 10^{-1}$ $\mu{\rm m}^2$, $A_0\phi \sim 10^{-5}\,{\rm s}^{-1}$ inferred in our previous study [7] from experimental data on the endocytic sorting of low-density lipoproteins, one obtains $N \ll 10^3$. Therefore, the analytical estimate (19), based on our phenomenological theory of sorting, suggests that a large number of protein cargos of different species may in principle be distilled in parallel on a cell membrane. It is worth observing, however, that Eq. (19) can provide only a qualitative indication about the breakdown of the low-density regime, as it was derived neglecting the contribution of complicated logarithmic prefactors [7]. The onset of the regime of molecular crowding will be therefore more precisely investigated in the next section by means of numerical simulations of a lattice-gas implementation of the sorting process.

The ordering effect of the sorting process on the molecule gas can be quantified as follows. Consider the case where molecule injection takes place by the fusion into a membrane system of area A of vesicles carrying a well-mixed cargo of molecules of all of the N distinct molecular species. In the steady state, the same number of cargo molecules is extracted in vesicles containing in average $\delta\mathcal{N}_i = A\,\phi_i\,\delta t$ molecules of only one of the ith molecular species. Formally treating empty membrane regions of area A_0 as a 0th molecular species, we define a corresponding flux density ϕ_0. The change in entropy due to the demixing process can then be measured as [33,34]:

$$\delta S = \sum_{i=0}^{N} \delta\mathcal{N}_i \log \frac{\delta\mathcal{N}_i}{\delta\mathcal{N}}, \tag{20}$$

with $\delta\mathcal{N} = \sum_{i=0}^{N} \delta\mathcal{N}_i$, resulting in a simple expression for the average rate of entropy production per unit membrane area:

$$\begin{aligned}\frac{1}{A}\frac{\delta S}{\delta t} &= \sum_{i=0}^{N} \phi_i \log \frac{\phi_i}{\phi_0 + \phi} \\ &= -\phi_0 \log\left(1 + \frac{\phi}{\phi_0}\right) - \phi \log\left(1 + \frac{\phi_0}{\phi}\right) - \phi \log N.\end{aligned}$$

III. NUMERICAL RESULTS

The sorting of a plurality of distinct molecular species is here further investigated by means of numerical simulations of a generalized version of the hard-core lattice-gas model previously introduced in Ref. [7]. A schematic representation of the stochastic processes taking place in the model is shown in Fig. 1. Cargo molecules are individually inserted on unoccupied sites of a lattice with rate k_I, and diffuse by hopping on unoccupied neighboring sites with rate k_D. The affinity between molecules of the same species induces a decrease in the mobility rate k_D by a factor g^{n_h}, where g is a microscopic measure of interaction strength, and n_h is the number of neighboring sites occupied by homotypic molecules. Molecules of different species are inserted in empty lattice sites with the same rate, and the only interaction between them is due to excluded volume effects. Areas are measured as multiples of the area A_0 of a lattice site. In the stationary state, the incoming flux per site is $\phi = k_I(1-\rho)$, where ρ is the stationary molecule density on the lattice. Connected homotypic domains that reach the size m are extracted from the system. Further details on the lattice-gas model are provided in Appendix A.

A. Sorting multiple molecular species

The results of numerical simulations of the model on a 100×100 square lattice with the realistic [7] parameter values $\phi/k_D = 10^{-5}$, $m = 25$, are displayed in Fig. 2. Consistent

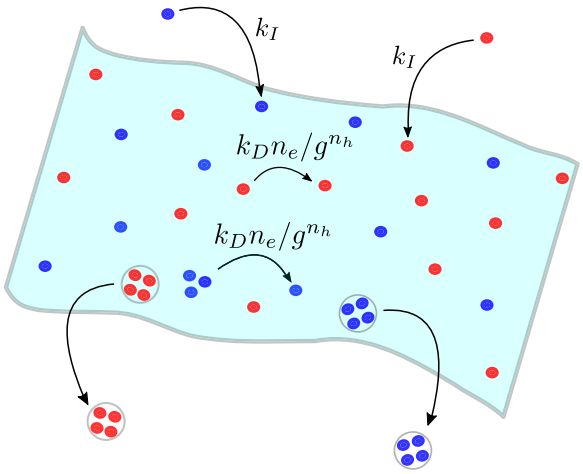

FIG. 1. Schematic representation of the hard-core lattice-gas model used to investigate the parallel sorting of multiple molecular species.

with previous results [7,8], Figure 2(a) shows that, in an intermediate range of values of the microscopic interaction strength g, the stationary density of molecules ρ exhibits a minimum, corresponding to an optimal sorting regime. Increasing the number N of sorted species, the optimal region moves towards larger values of g, indicating that efficient molecular sorting becomes more and more difficult to obtain as the number of sorted species increases. For very large N, molecular sorting can take place only in a restricted interval of values of g, as the system tends to freeze into an overcrowded state for both lower and higher values of g. The existence of a maximum value g_N such that sorting at $g > g_N$ becomes impossible for large N due to crowding effects can also be checked by looking at the behavior of the stationary molecular density $\rho_{g=\infty}$ as a function of N [Appendix B, Fig. 7(a)]: This density rapidly transitions to values of order 1 (high molecular crowding) for $N \sim 10$, signaling that sorting is strongly impaired at high g for $N \gtrsim 10$.

When $N \sim 10$, sorting is still possible around the optimal region, which, however, tends to shrink progressively with increasing N, since, as seen in the previous section, the optimal molecular density $\rho_{\rm opt}$ grows with N, in quantitative agreement with the scaling law $\rho_{\rm opt} \sim N^{1/2}$ predicted by the phenomenological theory [Fig. 2(b)]. The deviation from the $N^{1/2}$ scaling observed at $N \sim 10^2$ signals the breakdown, even at optimality, of the low-density regime where the parallel processes of sorting of different species take place approximately independently of each other. For larger N, sorting domains are no longer well separated and molecular mobility is strongly reduced [Appendix B, Fig. 7(b)]. The behavior of the interdomain half distance L, numerically evaluated as a function of g for various values of N, is displayed in Fig. 2(e). The shaded area represents the region where the ratio of L to the extraction size $A_E^{1/2}$ is smaller than 1. This region corresponds to a crowding regime where the different species hinder the mobility of each other, thus reducing the sorting efficiency. This is qualitatively confirmed by observing the snapshots of configurations obtained from simulations of the lattice-gas model for different values of N, where the existence of two

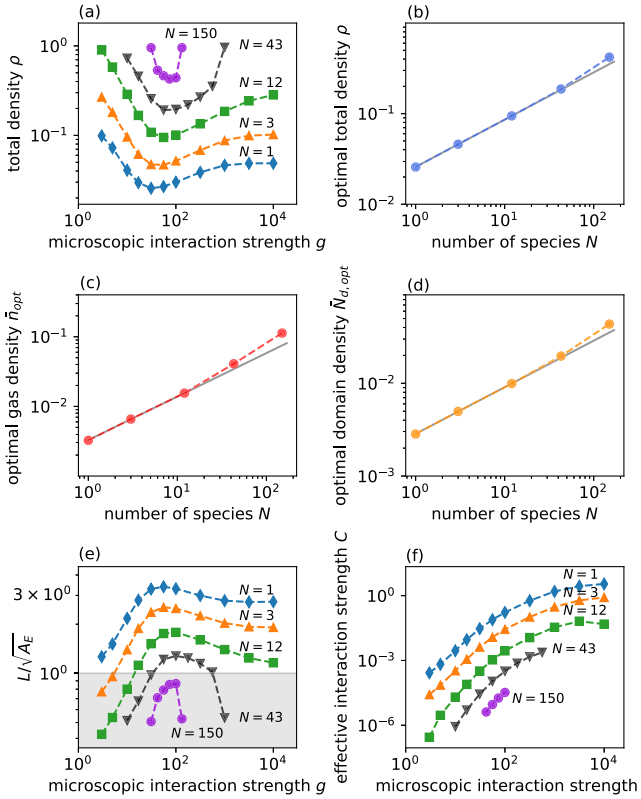

FIG. 2. (a) Total molecule density as a function of the microscopic interaction strength g, for increasing values of the number of species N. For large N, sorting remains possible only in a restricted interval of values of g. [(b)–(d)] Total molecule density, density of freely diffusing molecules, and density of domains, respectively, as functions of the number N of sorted molecular species, in the optimal sorting regime. The solid lines are fitted with $\rho \sim N^a$, $\bar{n} \sim N^b$, and $\bar{N}_d \sim N^c$ with $a = 0.51$, $b = 0.62$, $c = 0.50$. These scaling relations are verified for $N < 20$, whereas, in qualitative agreement with the theory, increasing deviations are observed for larger N. (e) Ratio of the interdomain half-distance L to the extraction size $A_E^{1/2}$ as a function of the microscopic interaction strength g. The parameter region where the system becomes overcrowded and sorting is impaired is marked in light gray. (f) Effective interaction strength C as a function of the microscopic interaction strength g for different values of the number of molecular species N. Simulations were performed at fixed incoming molecule flux $\phi/k_D = 10^{-5}$ on a square lattice.

different regimes, a low-density one and a crowded one, can be clearly distinguished (Fig. 3). A convenient measure of the mutual affinity of homotypic molecules, both in a dilute and in a crowded environment, is the effective, macroscopic interaction strength C, which can be computed by inverting Eqs. (4) and (7) [7,8]. Figure 2(f) shows that C increases monotonically as a function of the microscopic interaction strength g (as previously observed for $N = 1$ in Ref. [8]), but decreases monotonically for increasing N, as predicted by the phenomenological theory. Altogether, these numerical results suggest that up to 10–100 distinct protein cargos might in principle be sorted in parallel, with the highest value attainable only in the optimal regime, while strong crowding effects are expected to impair molecular sorting for larger values of N.

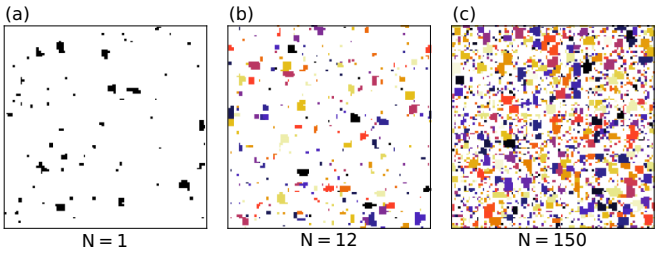

FIG. 3. Snapshots of the sorting process for increasing values of the number of species N (from left to right). Different molecular species have been marked with different colors (shades of gray). Simulations were performed in the optimal regime at the realistic value $\phi/k_D = 10^{-5}$ of the incoming molecule flux.

B. Sorting species with different mutual affinities

For the symmetric case, where all the molecular species have similar mutual affinities, we found simple scaling laws for the molecular density at the steady state in the optimal region, away from the crowding regime. It is then interesting to investigate to which extent this symmetry requirement is restrictive. To this aim, we here consider the process of sorting of $N = 2$ molecular species, such that their mutual affinities are characterized by independent, and possibly different microscopic interaction strengths g_1 and g_2 (see Appendix A for the definition of the lattice-gas model when $g_1 \neq g_2$). By measuring the stationary molecule density ρ, one may look for a global minimum as a function of the two interaction strengths. Figure 4 shows the existence of a single global minimum of the total molecule density ρ for $g_1 = g_2 = g_{\rm opt}$, suggesting that molecular sorting may be most efficient when the distinct sorted molecular species have similar homotypic affinities, and that the symmetry requirement imposed in the previous treatment may be not too restrictive, as far as the optimal sorting regime is concerned.

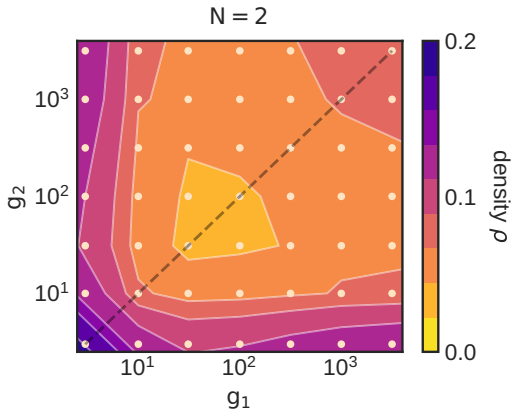

FIG. 4. Optimal sorting of two distinct molecular species (lighter region) is obtained for equal homotypic affinities (dashed line $g_1 = g_2$). Simulations were performed at fixed incoming molecule flux $\phi/k_D = 10^{-5}$ on a square lattice. Dots correspond to computed values of ρ, level curves are obtained by linear interpolation of the computed values.

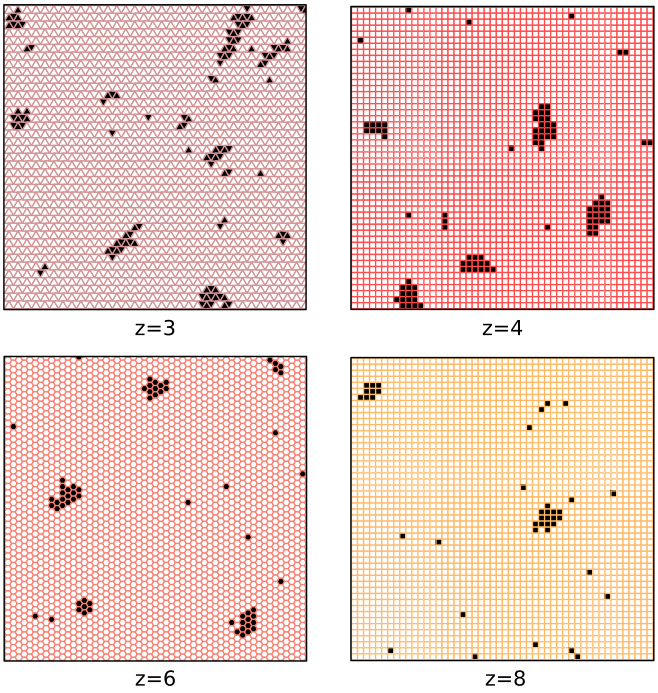

FIG. 5. Snapshots of simulated optimal sorting of $N = 1$ molecular species with incoming molecule flux $\phi/k_D = 10^{-5}$ on regular lattices with different coordination number z and equal area A_0 of the elementary lattice site. The panels show enlargements of one quarter of the total system.

C. Sorting multivalent molecules

An increasing amount of evidence suggests that a crucial factor in a variety of intracellular phase separation processes is valence, which may be defined as the average number of interacting neighbors of a molecule in a phase-separated domain [25,26,35]. Experiments have shown that multivalence promotes domain stability [25,36], and that multivalent protein interactions are responsible for the assembly of endocytic sorting domains [37].

A simple way to investigate the role of valence in the present numerical framework is to consider the diffusion of molecules on regular lattices with different coordination numbers z, i.e., on triangular, square, and hexagonal lattices ($z = 3, 4, 6$) (Fig. 5). The $z = 8$ case can be implemented by considering the square lattice where nearest neighbors along the diagonals are considered in addition to nearest neighbors along the horizontal and vertical directions. In this lattice-gas framework, the lattice coordination number z can be treated as a proxy of molecular valence. In order to correctly compare the sorting dynamics on lattices with different coordination numbers, the microscopic rates were chosen in such a way to provide the same macroscopic diffusive dynamics in the continuum limit for all $z = 3, 4, 6, 8$ (see Appendix C). To focus on the dependence of the sorting process on z, the analysis is restricted to the case where a single molecular species is sorted ($N = 1$).

Figure 6(a) shows that higher valence implies larger values of the effective, macroscopic interaction strength C at fixed values of the microscopic interaction strength g, consistent with the intuition that molecules of higher valence can more

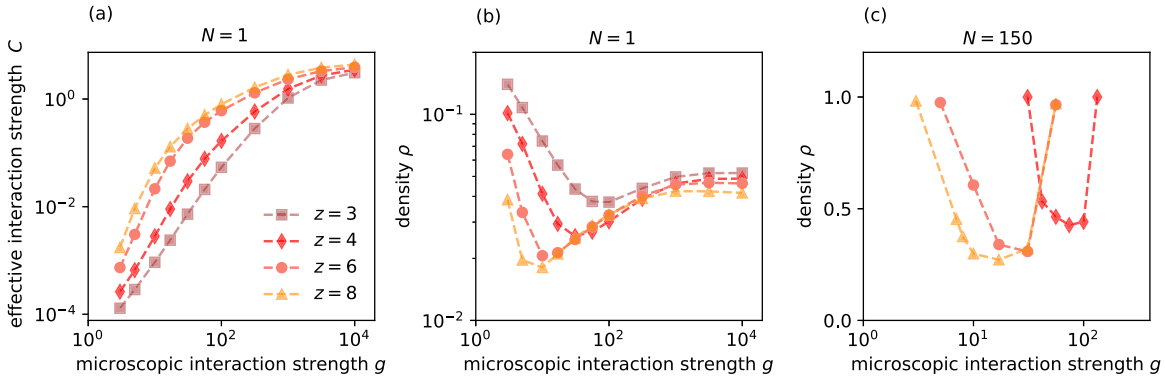

FIG. 6. (a) Effective interaction strength C as a function of the microscopic interaction strength g and of the valence z. Higher values of z compensate for smaller g. (b) Total molecule density ρ as a function of the microscopic interaction strength g for different values of the valence z. (c) Density ρ as a function of the interaction strength g for different values of the valence z in a system with $N = 150$ molecular species. Simulations were performed with $\phi/k_D = 10^{-5}$.

easily aggregate and form phase-separated domains, and that higher valence can compensate for smaller values of the microscopic aggregation strength. This tendency is confirmed by Fig. 6(b), showing that optimal sorting (corresponding to the minima of the density curves) is realized at lower values of the microscopic interaction strength g for increasing z. Interestingly, the corresponding optimal values of the stationary molecule density ρ also decrease for increasing z. Perhaps even more importantly, Fig. 6(c) shows that the interval of values of g such that the sorting process can take place for high N (here $N = 150$) significantly widens for increasing z: In this condition, sorting is impossible for $z = 3$ due to molecular crowding, but is instead possible over more then a decade of g values for $z = 6, 8$.

Altogether, these numerical results show that, at least in the present, highly simplified modeling framework, higher valence promotes more efficient sorting. It is interesting to speculate that this may also be true in actual biological systems.

IV. CONCLUSION

Biological membranes host a sophisticated process of molecule sorting and demixing, which is essential for the formation and maintanence of the distinct chemical identies of diverse organelle and membrane regions. We suggested [7] that the main drivers of this hectic distillation process are the phase separation of molecules of distinct species driven by their mutual, direct [9,25,26] or indirect [10–16], interactions, and by the tendency of phase-separated molecular domains to induce membrane bending and vesicle nucleation [38]. Based on these assumptions, we have previously introduced a phenomenological theory of the process of sorting of a single molecular cargo [7,8]. Since molecular sorting is first of all a demixing process, it is interesting to generalize the theory to the case where $N > 1$ distinct molecular species are sorted in parallel. The present work is a step forward in this direction, in which we considered the simplest case where N molecular species of similar *effective* homotypic affinities are sorted simultaneously on the same membrane system. In this case, analytical arguments and numerical simulations of a hard-core lattice-gas model show that, when keeping fixed the total incoming molecular flux, the average molecule residence time and the average molecule density on the membrane system at the steady state increase with the heterogeneity N of the molecular pool as $N^{1/2}$. Simulations performed with biologically realistic parameter values suggest that a large number of distinct molecular species (of the order of 10–100, depending on the degree of optimality of the process) can be sorted in parallel on a given membrane system without significant crowding effects. The study of the $N = 2$ case for independent values of the mutual molecular affinities suggests that sorting may be most efficient when the distinct molecular species have similar homotypic affinity. Lastly, motivated by the crucial role of multivalent molecules in driving biological phase separation [25,26,35], we analyzed the effect of valence on the sorting process by simulating our sorting model on regular lattices of varying coordination number, finding that, in this framework, higher valence allows for more efficient sorting of a large number of distinct molecular species over a larger interval of mutual interaction strengths.

Here we have adopted a coarse-grained approach where for simplicity a single, representative molecular species, or cargo, is assumed to accumulate in each sorting domain. It should be understood, however, that in a real cell, sorting domains contain, along with the sorted cargo, also a large number of other molecules that contribute to the localization process, often as part of reinforcing feedback loops. So, for instance, in clathrin-mediated endocytosis the sorting of a cargo molecule is accompanied by the concurrent accumulation of auxiliary molecules such as clathrin, AP-2, Fcho1/2, and Eps15 that are part of a complex network of interactions, involving both the sorted cargo and specific membrane lipids such as PIP2 [30,37,39]. In recycling endosomes, sorting domains are characterized by the presence of Rab11, Rab5, and associated activatory and inhibitory factors (GEFs and GAPs), participating in multiple feedback loops that also involve specific membrane lipids [17,40]. The assembly sites of influenza virions are self-organized domains enriched in hemagglutinin, neuramidase, and other proteins that are part of an interaction network including specific lipid factors arranged in a liquid-ordered phase [4,41]. A similar scenario is observed in HIV assembly sites, where several structural proteins, such as Gag, self-organize in protein-lipid domains characterized by an abundance of liquid-ordered lipids that in their turn favor the

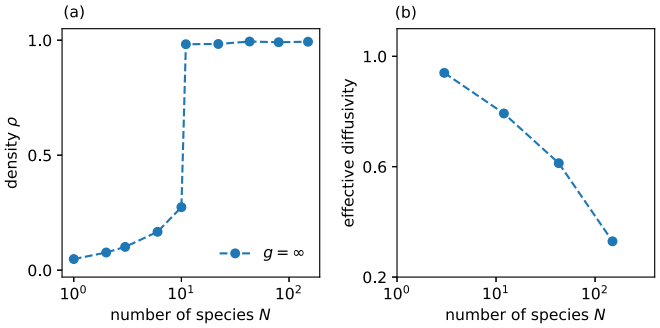

FIG. 7. (a) Total molecule density ρ as a function of the number of species N in the limit case $g = \infty$. Above a critical value $\sim$10 of the number of species, the density becomes $\sim$1, signaling that most lattice sites are filled and that the distillation process has come to a stop due to molecule overcrowding. (b) The effective diffusivity of a test particle decreases as the number of species N increases, signaling that molecular mobility is strongly reduced. Simulations were performed at fixed incoming molecule flux $\phi/k_D = 10^{-5}$ on a square lattice.

recruitement of more Gag molecules [5,42,43]. In all of these cases, measurable phenomenological quantities that may be used to check the validity of our theoretical and numerical predictions include the lateral diffusivity of each representative sorted cargo, the average density of such cargos in sorting domains, the flux of sorted cargo molecules in the steady state, and the average surface density of cargo molecules and of sorting domains. While the low level of molecular detail included in our abstract theory does not allow for significant predictions of the absolute values of such quantities, it would be interesting to check whether the predicted scaling laws are compatible with the experimental dependence of the relevant quantities on the number of distinct, simultaneously sorted cargo species.

ACKNOWLEDGMENTS

We gratefully acknowledge useful discussions with Guido Serini, Carlo Campa, Igor Kolokolov, and Vladimir Lebedev. Numerical calculations were made possible by a SmartData@PoliTO agreement providing access to BIGDATA high-performing computing resources at Politecnico di Torino, and by a CINECA-INFN agreement providing access to resources on MARCONI at CINECA.

APPENDIX A: LATTICE-GAS MODEL

The molecular sorting process described in the main text is implemented in terms of a lattice-gas model, where molecules of multiple species are distributed on a two-dimensional regular lattice with periodic boundary conditions. Each lattice site can host a single molecule at most, but there is no limit to the number of species that can populate the lattice. The current state of the system is described by a multivariate configuration where 0 marks an empty lattice site, while a number $i \in \{1, \ldots, N\}$ marks a molecule of the ith species residing on a given site. The state of the system evolves according to a continuous-time Markov chain consisting of the following three processes: (1) molecules, whose species

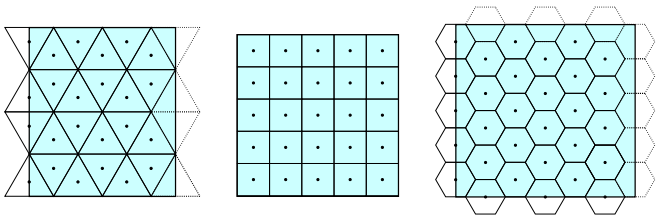

FIG. 8. Small periodic regular lattices with $z = 3, 4, 6$, with identical area A_0 of the elementary lattice site and approximately equal total area (light blue shaded region). The centers of the sites belonging to each lattice are marked with a black dot.

are chosen randomly from a set of N species in such a way that the overall flux has the assigned value ϕ, are inserted into empty sites with rate k_I; (2) molecules jump towards empty neighboring sites with rate $k_D n_e / g_i^{n_h}$, where n_e is the number of empty neighboring sites, g_i is the intermolecular interaction strength between molecules belonging to the ith species, with $i = 1, \ldots, N$, and n_h is the number of homotypic molecules in neighboring sites; and (3) the molecules in a connected domain of homotypic molecules are extracted when the domain reaches the extraction size m. (The extraction mechanism adopted here is a slightly simplified version of the one used in Ref. [7], where the molecules of a connected domain were extracted only when the domain grew to the point of containing a molecule-filled square of given size.) A schematic representation of these mechanisms is shown in Fig. 1. In the simulations, $A_0 = 1$, i.e., areas are measured as multiples of the elementary lattice area A_0, and the realistic value $m = 25$ is used. In this way, the relevant microscopic parameters describing the process are the intermolecular interaction strength g, valence z, and ratio k_I/k_D. For low values of the molecule density ρ, such as those experimentally measured in Ref. [7], the molecule flux $\phi = k_I(1 - \rho)$ is approximately equal to the insertion rate k_I. Compatibly with experimental observations [7], simulations were performed with $\phi/k_D = 10^{-5}$.

APPENDIX B: CROWDING EFFECTS

The deviation from the $N^{1/2}$ scaling observed at large N in Fig. 2(b) is a consequence of the breakdown of the low-density regime where the processes of sorting of the different molecular species are approximately independent [Fig. 7(a)]. For large N, the sorting domains are no longer well separated, and molecular mobility is strongly reduced. This can be checked by tracking the diffusive motion of a test molecule which does not interact with any of the molecules of the $i = 1, \ldots, N$ species, except for excluded volume effects. The effective diffusivity of the test molecule, measured empirically from the temporal growth of its mean-squared displacement, is observed to decrease when the number N of molecular species increases [Fig. 7(b)].

APPENDIX C: RELATION BETWEEN MICROSCOPIC AND MACROSCOPIC DIFFUSIVITIES

The microscopic rate k_D of jump to an empty neighboring site of the lattice can be related to the macroscopic diffusivity D as follows. Consider the diffusion of a single molecule on

an otherwise empty lattice, and let $n_x(t)$ be the probability that the molecule occupies site x at time t. At time $t + \delta t$,

$$n_x(t + \delta t) = n_x(t) + k_D\, \delta t \cdot \sum_{y \in \partial x} (n_y - n_x), \qquad \text{(C1)}$$

where ∂x is the set of nearest neighbors of x. For the regular lattices with $z = 3, 4, 6$, expanding n_y in a Taylor series centered in x and dividing by δt, Eq. (C1) tends to the diffusion equation for n_x, with $D = \frac{1}{4}\, z\, k_D\, d^2$, where z is the number of nearest neighbors of x, and d is the distance between the center of neighboring sites. The same procedure applied to the $z = 8$ case with diagonal neighbors gives instead $D = 3\, k_D\, d^2$. For a correct comparison of the sorting dynamics in the presence of different coordination numbers, regular lattices of different coordination number but identical area A_0 of the elementary lattice site (i.e., of identical area per molecule) were used (Fig. 8). The total area of each lattice was chosen to contain approximately 100^2 sites, and the microscopic jump rate k_D was rescaled to provide the same value of the macroscopic diffusivity D for all $z = 3, 4, 6, 8$.

[1] I. Mellman and W. J. Nelson, Nat. Rev. Mol. Cell Biol. **9**, 833 (2008).
[2] S. Sigismund, S. Confalonieri, A. Ciliberto, S. Polo, G. Scita, and P. P. Di Fiore, Physiol. Rev. **92**, 273 (2012).
[3] O. Pornillos, J. E. Garrus, and W. I. Sundquist, Trends Cell Biol. **12**, 569 (2002).
[4] J. S. Rossman and R. A. Lamb, Virology **411**, 229 (2011).
[5] P. Sengupta and J. Lippincott-Schwartz, Viruses **12**, 745 (2020).
[6] B. B. Motsa and R. V. Stahelin, Bioch. Soc. Trans. **49**, 1633 (2021).
[7] M. Zamparo, D. Valdembri, G. Serini, I. V. Kolokolov, V. V. Lebedev, L. Dall'Asta, and A. Gamba, Phys. Rev. Lett. **126**, 088101 (2021).
[8] E. Floris, A. Piras, F. S. Pezzicoli, M. Zamparo, L. Dall'Asta, and A. Gamba, Phys. Rev. E **106**, 044412 (2022).
[9] S. F. Banani, H. O. Lee, A. A. Hyman, and M. K. Rosen, Nat. Rev. Mol. Cell Biol. **18**, 285 (2017).
[10] A. Gamba, A. de Candia, S. Di Talia, A. Coniglio, F. Bussolino, and G. Serini, Proc. Natl. Acad. Sci. USA **102**, 16927 (2005).
[11] K. John and M. Bär, Phys. Rev. Lett. **95**, 198101 (2005).
[12] A. Gamba, I. Kolokolov, V. Lebedev, and G. Ortenzi, Phys. Rev. Lett. **99**, 158101 (2007).
[13] M. Semplice, A. Veglio, G. Naldi, G. Serini, and A. Gamba, PLoS ONE **7**, e30977 (2012).
[14] M. Zamparo, F. Chianale, C. Tebaldi, M. Cosentino-Lagomarsino, M. Nicodemi, and A. Gamba, Soft Matter **11**, 838 (2015).
[15] J. Halatek, F. Brauns, and E. Frey, Phil. Trans. R. Soc. B: Biol. Sci. **373**, 20170107 (2018).
[16] E. Floris, A. Piras, L. Dall'Asta, A. Gamba, E. Hirsch, and C. C. Campa, Comp. Struct. Biotechn. J. **19**, 3225 (2021).
[17] A. Cezanne, J. Lauer, A. Solomatina, I. F. Sbalzarini, and M. Zerial, eLife **9**, e54434 (2020).
[18] X. Wang, Z. Chen, M. Mettlen, J. Noh, S. L. Schmid, and G. Danuser, eLife **9**, e53686 (2020).
[19] S. Rodriguez-Gallardo, K. Kurokawa, S. Sabido-Bozo, A. Cortes-Gomez, A. Ikeda, V. Zoni, A. Aguilera-Romero, A. M. Perez-Linero, S. Lopez, M. Waga *et al.*, Sci. Adv. **6**, eaba8237 (2020).
[20] S. Rodriguez-Gallardo, K. Kurokawa, S. Sabido-Bozo, A. Cortes-Gomez, A. M. Perez-Linero, A. Aguilera-Romero, S. Lopez, M. Waga, A. Nakano, and M. Muñiz, PLoS ONE **16**, e0258111 (2021).
[21] Y. Shimizu, J. Takagi, E. Ito, Y. Ito, K. Ebine, Y. Komatsu, Y. Goto, M. Sato, K. Toyooka, T. Ueda *et al.*, Nat. Commun. **12**, 1901 (2021).
[22] N. Gomez-Navarro and E. Miller, J. Cell Biol. **215**, 769 (2016).
[23] N. Destainville, Europhys. Lett. **91**, 58001 (2010).
[24] N. Meilhac and N. Destainville, J. Phys. Chem. B **115**, 7190 (2011).
[25] P. Li, S. Banjade, H.-C. Cheng, S. Kim, B. Chen, L. Guo, M. Llaguno, J. V. Hollingsworth, D. S. King, S. F. Banani *et al.*, Nature (London) **483**, 336 (2012).
[26] S. Banjade and M. K. Rosen, eLife **3**, e04123 (2014).
[27] S. Banjade, L. Zhu, J. R. Jorgensen, S. W. Suzuki, and S. D. Emr, Sci. Adv. **8**, eabm5149 (2022).
[28] E. Lifshitz and L. Pitaevskii, Physical Kinetics, *Course of Theoretical Physics* (Pergamon Press, New York, 1981), Vol. 10.
[29] V. V. Slezov, *Kinetics of First Order Phase Transitions* (John Wiley & Sons, Weinheim, 2009).
[30] M. Kaksonen and A. Roux, Nat. Rev. Mol. Cell Biol. **19**, 313 (2018).
[31] T. Kirchhausen, D. Owen, and S. C. Harrison, Cold Spring Harb. Perspect. Biol. **6**, a016725 (2014).
[32] M. Zamparo, L. Dall'Asta, and A. Gamba, J. Stat. Phys. **174**, 120 (2019).
[33] L. D. Landau and E. M. Lifshitz, *Statistical Physics—Part 1* (Pergamon Press, New York, 1980).
[34] G. B. Brandani, M. Schor, C. E. MacPhee, H. Grubmüller, U. Zachariae, and D. Marenduzzo, PLoS ONE **8**, e65617 (2013).
[35] Y. Shin and C. P. Brangwynne, Science **357**, eaaf4382 (2017).
[36] S. F. Banani, A. M. Rice, W. B. Peeples, Y. Lin, S. Jain, R. Parker, and M. K. Rosen, Cell **166**, 651 (2016).
[37] K. J. Day, G. Kago, L. Wang, J. B. Richter, C. C. Hayden, E. M. Lafer, and J. C. Stachowiak, Nat. Cell Biol. **23**, 366 (2021).
[38] P. Bassereau, R. Jin, T. Baumgart, M. Deserno, R. Dimova, V. A. Frolov, P. V. Bashkirov, H. Grubmüller, R. Jahn, H. J. Risselada *et al.*, J. Phys. D: Appl. Phys. **51**, 343001 (2018).
[39] L. Ma, P. K. Umasankar, A. G. Wrobel, A. Lymar, A. J. McCoy, S. S. Holkar, A. Jha, T. Pradhan-Sundd, S. C. Watkins, D. J. Owen, and L. M. Traub, Dev. Cell **37**, 428 (2016).
[40] C. C. Campa, J. P. Margaria, A. Derle, M. D. Giudice, M. C. D. Santis, L. Gozzelino, F. Copperi, C. Bosia, and E. Hirsch, Nat. Chem. Biol. **14**, 801 (2018).
[41] G. P. Leser and R. A. Lamb, J. Virol. **91**, e02104-16 (2017).
[42] C. Favard, J. Chojnacki, P. Merida, N. Yandrapalli, J. Mak, C. Eggeling, and D. Muriaux, Sci. Adv. **5**, eaaw8651 (2019).
[43] J. Podkalicka and P. Bassereau, Nat. Cell Biol. **21**, 413 (2019).